Classical and Quantum Dynamics of the O + CN Reaction

Erik Abrahamsson

För avläggande av teknologie licentiatexamen i kemi med inriktning mot fysikalisk kemi, som presenteras och examineras vid ett seminarium fredagen den 24 mars 2006, kl 10:15 i sal KB, Kemigården 3, Göteborg

Examinator: Professor Sture Nordholm
Granskare: Associate Professor Kim Bolton, Göteborgs Universitet

Classical and Quantum Dynamics of the O + CN Reaction

Erik Abrahamsson
Department of Chemistry, Physical Chemistry
Göteborg University
SE-412 96 Göteborg, Sweden

Abstract

In this work the reaction of ground state oxygen atoms, $O(^3P)$, with ground state cyanogen radicals, $CN(X^2\Sigma^+)$ is investigated. The reaction has received attention as a possible major source of depletion of CN in both combustion and in dense interstellar clouds. Electronic structure (CASPT2) calculations have been performed for the lowest $^2\Pi$ and $^4\Sigma^-$ states of the NCO system. Furthermore, spin-orbit coupling terms between the two surfaces have been calculated using RASSI with CASSCF wave functions as basis set. Time-dependent wave packet and quasiclassical trajectory calculations are presented for the two surfaces, both with and without coupling between them. The $^2\Pi$ surface has an almost 6 eV deep potential well, making the wave packet calculations a challenge. Generally the agreement is good between the methods, as would be expected, but some notable differences are found. These are the first reported quantum dynamics calculations for this reaction.

Preface

This licentiate thesis is based on and serves as an introductory text to the two research papers listed below, henceforth referred to as Paper I and Paper II. The work has been carried out at the Department of chemistry, Physical chemistry, Göteborg University under the supervision of professor Gunnar Nyman, Göteborg University, and associate professor Nikola Marković, Chalmers University of Technology.

I. **Classical and quantum dynamics of the O + CN reaction**
Erik Abrahamsson, Stefan Andersson, Nikola Marković and Gunnar Nyman
Article accepted for publication in *Chem. Phys.*

II. **Dynamics of the O + CN reaction on two coupled surfaces**
Erik Abrahamsson, Stefan Andersson, Nikola Marković and Gunnar Nyman
Manuscript.

Contents

Chapter 1

Introduction

The study of reaction dynamics is the study of *how* and *why* chemical reactions occur, at a molecular level. A chemical reaction is, usually, but not always, an effect of two (or more) molecules colliding, sometimes called a scattering process. The collision can result in a chemical reaction, that is, the breaking and forming bonds and the formation of new molecules. It can also be a non-reactive scattering process, where the molecules collide, transfer energy between each other and move away again, perhaps in new electronic, vibrational or rotational states. In this thesis we are concerned with bimolecular reactions, or rather, a diatomic molecule colliding with an atom. This might seem like a very trivial process, as it only involves three atoms, but as will be seen, it is highly complex.

Reaction dynamics can be studied experimentally, with high-precision instruments. It is also the interest of theoretical studies, trying to predict or explain experimental results, or find answers that cannot be obtained by experiments. The present work is all about theoretical calculations on a specific reaction – the reaction of an oxygen atom colliding with a cyanogen radical. The methods used to study the dynamics of the reaction are classical trajectories and quantum mechanical wave packet dynamics.

A simplified and intuitive view of classical trajectory dynamics can be to think of it as launching a marble into a labyrinth, studying the path it takes. Then the labyrinth would represent the potential energy of the system, and each marble the chemical system. By releasing a large swarm of marbles - trajectories - statistical conclusions can be drawn from their final state - their velocities and directions.

Wave packet dynamics is very similar in nature, but due to the Heisenberg uncertainty principle we cannot talk about marbles with known velocity and position. Instead we send a wave, represented by a wave packet that is distributed both in position and velocity, through the labyrinth. We never

really know exactly where it is and how fast it is moving, we can only determine its probability distribution. Governed by the Schrödinger equation, the wave packet can pass through walls - tunnel through barriers - and interfere with itself, creating resonances, phenomena not seen in the classical model.

Chapter 2

Background

2.1 Strategy

The general strategy when performing time-dependent reaction dynamics calculations is to first create the electronic potential energy surface (PES) on which the reaction takes place. The potential energy surface can be created beforehand for the entire multidimensional space - a global potential energy surface, or it can be created locally where needed in each time step, as done in direct dynamics. The potential energy surface can also be restricted to a specific symmetry, or specific geometries - known as reduced dimensionality. The surface can be created from experimental data, semi-empirical models or high level ab initio calculations. But no matter the choice, time-dependent scattering calculations cannot be performed without knowing the potential energy.

After the potential energy surface has been determined, the time-dependent dynamics of the reaction can be studied. The dynamics can be studied classically or quantum mechanically, on one potential energy surface, or on several coupled surfaces at once. Finally, the reaction has to be analyzed, by studying reaction probabilities, reaction times, lifetimes of formed complexes, and the energy distribution among the products.

This licentiate thesis continues by giving the background to this study, presenting some of the previous work on the NCO system. In Chapter 3 an overview of ab initio electronic structure calculations, from Hartree-Fock theory to multi-configurational perturbation theory, is given. Different methods to create an electronic potential energy surface from the ab initio energy points are presented, and the chapter ends by introducing the spin-orbit coupling.

In Chapter 4 the theoretical foundations for the time-dependent dynam-

ics are laid down. Quasi-classical trajectories (QCT) are presented, as well as trajectory surface hopping (TSH). The chapter continues with a discussion on time-dependent wave packet calculations. Attention is given to initiation, propagation, damping, and analysis of the wave packet, as well as propagation on coupled surfaces.

A brief summary of the included Paper I and Paper II is given in Chapter 5. Finally, Chapter 6 lets us glance into the future, revealing what might come ahead.

2.2 The NCO system

The triatomic system consisting of carbon, nitrogen, and oxygen (known as the CNO or NCO system) has been the focus of many experimental and theoretical studies during the last four decades. The reason for this is the combustion of atomic carbon. By understanding the process of carbon combustion in a nitrogen and oxygen containing atmosphere, the combustion process can be optimized and the release of unwanted byproducts, like NO_X, minimized. It is no wonder then, that it is the reaction C + NO that has by far received the most attention (see e.g. [1, 2] and references therein). There are numerous experimental studies of the reaction, as well as theoretical studies of both the dynamics and kinetics of the reaction.

The system is also of interest in astrophysics, as for example the CN radical is a known precursor to more complex molecules. Detailed understanding on the NCO system at very low temperatures could give considerable insight of the chemical evolution in dense interstellar clouds [3–7].

Several quasiclassical trajectory calculations (see [1, 2]) have been done for the C+NO reaction, as well as 2D [8] and 3D [9] wave packet dynamics. In the 3D calculations a PES containing the linear CNO minimum but not the deeper NCO minimum was used, which made the 3D study possible for a total angular momentum of zero. Recently 2D wave packet calculations for the collinear C+NO → CN+O reaction has been performed [10].

The reaction between ground state oxygen atoms with cyanogen radicals,

$$\mathrm{O}(^3\mathrm{P}) + \mathrm{CN}(\mathrm{X}^2\Sigma^+) \rightarrow \mathrm{CO}(\mathrm{X}^1\Sigma^+) + \mathrm{N}(^2\mathrm{D}), \tag{2.1}$$

and

$$\mathrm{O}(^3\mathrm{P}) + \mathrm{CN}(\mathrm{X}^2\Sigma^+) \rightarrow \mathrm{CO}(\mathrm{X}^1\Sigma^+) + \mathrm{N}(^4\mathrm{S}), \tag{2.2}$$

has not received as much attention. The reaction is believed to be a major source of depletion of CN in both dense interstellar clouds [3, 4] and combustion [11]. Detailed studies of the reaction were performed in the 1970's by

Schmatjko and Wolfrum, involving both quasiclassical trajectory (QCT) calculations on empirical LEPS type potential energy surfaces and experimental investigations of the dynamics and kinetics [12, 13]. From their room temperature experiments they concluded that about 20% of the reactive events produced $CO(X^1\Sigma^+) + N(^4S)$, corresponding to reaction (2.2) above.

Statistical adiabatic channel model (SACM) calculations have been published on the rate coefficients of reaction (2.1) at $T = 300 - 5000$ K [14]. We have also performed QCT calculations for the rate coefficients on the same reaction for T between 5 and 5000 K using ab initio based potential energy surfaces [2]. Apart from the mentioned QCT and SACM calculations, no computational studies have previously been published on the dynamics of these reactions.

Chapter 3

Potential Energy Surfaces

3.1 The Born-Oppenheimer Approximation

The foundation of this work is the non-relativistic Schrödinger equation, presented in 1926. The Schrödinger equation is a wave equation describing the behavior of matter, and is one of the corner stones in the theory of quantum mechanics. Solving the Schrödinger equation is a formidable task, and a series of approximations are usually made. When calculating the energies of atoms and molecules, it is generally assumed that the atoms are stationary, and the time-independent Schrödinger equation is used. In 1927 the Born-Oppenheimer approximation was presented. Due to the large mass ratio between the atom and the electron (the ratio of proton and electron masses is approximately 1836), the movement of the electrons is correspondingly faster than that of the atoms. Born and Oppenheimer made the assumption that the movement of the electron will adjust instantaneously to changes in nuclear configuration. Thus the Schrödinger equation can be separated into an equation defining the nuclear repulsion and an electronic Schrödinger equation describing the electron-electron and the electron-nuclear interactions. The Born-Oppenheimer approximation is fundamental to both electronic structure theory and to molecular dynamics, second in importance only to the Schrödinger equation itself, as it allows for the construction of potential energy surfaces.

The electronic Schrödinger equation can be written as

$$\hat{H}_{\text{el}}\Psi_{\text{el}} = E_{\text{el}}\Psi_{\text{el}} \tag{3.1}$$

where

$$\hat{H}_{\text{el}} = -\frac{1}{2}\sum_{i}\nabla_i^2 - \sum_{i,A}\frac{Z_A}{r_{iA}} + \sum_{i>j}\frac{1}{r_{ij}} \tag{3.2}$$

is the electronic Hamiltonian, expressed in atomic units. Here r_{iA} is the distance between electron i and atom A, r_{ij} is the distance between electron i and j, Ψ_{el} is the electronic wave function, and E_{el} is the electronic energy for a given nuclear geometry. The total energy, or the potential energy, of the system is thus the sum of the electronic energy E_{el} and the nuclear-nuclear repulsion:

$$V(\mathbf{R}) = E_{\text{el}}(\mathbf{R}) + \sum_{A,B} \frac{Z_A Z_B}{R_{AB}}, \tag{3.3}$$

where $\mathbf{R}$ is the nuclear positions and R_{AB} is the distance between nuclei A and B. This chapter is dedicated to solving the electronic Schrödinger equation, Eq. 3.1, and finding the electronic potential energy $V(\mathbf{R})$.

3.2 The Hartree-Fock Method

The Hartree-Fock method has, at least before the quite recent acceptance of density functional theory (DFT), been *the* method of choice when performing quantum chemistry. In Hartree-Fock theory, the electron-electron interaction is approximated by assuming that each electron moves in an average electric field created by all other electrons. This way the explicit electron-electron interaction is neglected, and Eq. 3.1 is reduced to a series of coupled differential equations, each only involving one electron. This allows the construction of Fock operators, which act as effective Hamiltonians for the electrons.

The Fock operators depend on all orbitals, forcing the solution to be known before the Hartree-Fock equations can be solved. Thus, the Hartree-Fock equations have to be solved by an iterative procedure, known as the self-consistent field (SCF) procedure. An initial guess is made as to the nature of the molecular orbital, the 'field', and the Hartree-Fock equations are solved until the resulting orbitals do not change (significantly) between iterations, i.e. the Fock operator is consistent with itself.

The Hartree-Fock method has the advantage of being relatively fast compared to many other methods, and generally producing results that at least give trends that follow experimental results. The main drawback of the Hartree-Fock method is the inability to account for correlation energy. The correlation energy is usually separated into two parts: a *dynamic* correlation, which is the effect of the cross-terms r_{ij}^{-1} in Eq. 3.2, and a *static* correlation. The observation of static correlation is an effect of the single determinant used in Hartree-Fock theory to describe the wave function. The correlation occurs when several separate electronic configurations are of near equal importance for describing the system, which cannot be accounted for by Hartree-Fock theory.

The correlation energy is usually defined as the difference between the Hartree-Fock limit (the HF energy with the largest effective basis set) and the true energy [15]. The correlation energy is generally not large, compared to the total energy, but to characterize properties such as chemical bonds, the difference between two energies is sought. Since this means taking the difference between two large numbers, the correlation may be of great importance. Correlation energy is also of great importance when studying open-shell systems - such as the NCO system.

Although the Hartree-Fock method has many drawbacks, it is still very important in nearly all ab initio calculations. Since it is reasonably accurate, and computationally cheap, the resulting wave functions serve as a perfect starting point for more accurate methods.

3.3 Perturbation Theory

Often it is possible to write the Hamiltonian of a problem that cannot easily be solved in two parts, one unperturbed (zeroth order) part that can easily be solved, and one part that represent a perturbation of the original problem. The most commonly used perturbation theory is the Møller-Plesset Perturbation Theory (MPPT), suggested by Rayleigh and Schrödinger, and applied in 1934 by the Danish scientists Møller and Plesset [16]. Second order Møller-Plesset perturbation theory (MP2) results in significant improvements over Hartree-Fock theory, and is relatively computationally cheap (first order MMPT - MP1 - results in the Hartree-Fock energy). Higher-order corrections can be made (MP3, MP4, etc) to improve the results by recovering more of the correlation energy. MP3 has no major advantage over MP2, and in practice only MP2 or MP4 are used [17].

The main advantages of MPPT are that it is both size-consistent and size-extensive, if the reference function is so [15]. This means that MPPT can be used to correctly represent chemical reactions. However, MPPT is not variational, and the energy calculated no longer has a lower bound in the exact value. This problem is generally quite small, and MPPT theory has gained widespread use.

3.4 Multi-Configurational Methods

Whereas MPPT methods can recover most of the dynamic correlation, it still cannot account for the static correlation that occurs when more than one electron configuration is of importance for describing the system. The

MPPT methods still rely on one determinant to describe the system, which is generally enough for most closed-shell system. But for open-shell systems, such as for example the NCO system studied here, the static correlation is large, and single configuration methods are inadequate to describe the system.

By exchanging the single configurational HF wave function with a sum over all probable configurations, the static correlation is accounted for. Within this sum, each configuration is given a weight (configuration interaction coefficients), which is optimized together with the orbitals. This is known as the multi-configurational self-consistent field (MCSCF) method. In practice, the length of the MCSCF expansion is finite and quite limited, due to the simultaneous optimization of the orbitals and CI coefficients. While the static correlation is at least partly determined by this method, choosing the proper set of configurations is problematic. To standardize the selection of configurations, the complete active space SCF (CASSCF) method [18] has been developed. In this method, the orbital space is divided into three subspaces: the *inactive*, *active*, and *secondary* orbital spaces. The inactive orbitals are orbitals that are always doubly occupied, typically the core orbitals, while the active orbitals are the valence orbitals, with no restrictions on the occupation number. Finally, the secondary orbitals are virtual orbitals that are always left unoccupied. CASSCF is not inherently size-consistent, but the active space can be chosen such that size-consistency is achieved. The upper limit for performing CASSCF calculations is for about 12-15 active orbitals, making the NCO system one of the largest systems that can be treated with all valence electrons in the active orbital space.

CASSCF is a zeroth order method, and even though the static correlation is recovered, the dynamic correlation, caused by the electron-electron repulsion, is not included. The CASPT2 (complete active space second-order Møller-Plesset) method is a multi-configurational reference function second-order perturbation method (see for example Ref. [15]). The CASSCF wave function, which contains the static correlation, is used as multi-configurational reference function for the MP2 method, which includes the dynamic correlation. CASPT2 is generally a very effective method for calculating a global potential energy surface.

A CASPT2 calculation is made in three steps: First a Hartree-Fock calculation is performed to give a starting wave function for the subsequence CASSCF calculation, in which the static correlation is retrieved. The CASSCF wave function is then used as reference function for the CASPT2 calculation, which is the third and final step.

3.5 Creating a Potential Energy Surface

Even today, despite the rapid improvement in both computer architecture and computational algorithms, ab initio calculations are still very computationally time-consuming, and dynamic calculations may demand hundreds of thousands, or even millions, of energy evaluations to be accurate. Thus, methods have been developed to accurately evaluate the potential energy between the ab initio energy points, allowing the creation of an arbitrary number of energy points from a limited set of ab initio calculations.

Usually about 10^N, where N is the number of independent coordinates, energy points are needed for an accurate description of the full potential energy surface. The energies at short ranges are preferably calculated by some ab initio method, like the ones described above. Calculations of the long-range interactions are usually simplified by approximating the wave function of the whole system (in our case a triatomic system) as the product of the wave function of the fragments (which in our case is a diatomic fragment and an atom). The electronic energies of the fragments are calculated separately, and the remaining interaction energy is calculated as the sum of electrostatic, induction and dispersion interaction energies. How this can be applied in the interaction between an atom and diatomic molecule is described in detail in [19].

To calculate the electronic potential energy in between the calculated energy points, various methods can be used. The oldest method has been to fit the energy points to a set of analytical functions. Common function types are LEPS (London-Eyring-Palanyio-Sato) [20] functions and MBE (many-body expansion) [21]. When fitting an analytical function to the energy points, the energy at the points is not reproduced exactly, but is optimized by means of a least square fit. Analytical fitting usually involves many unknown parameters, and the accuracy of the resulting surface depends on the choice of functional form, and requires skill and insight to produce an accurate potential energy surface.

In the last ten to fifteen years, different interpolation procedures for constructing potential energy surfaces have gained increased popularity. Interpolation methods reproduce the input energy points exactly, as opposed to the fitting procedures. However, it does not guarantee proper behavior between the grid points, where unphysical oscillations may occur. The review by Nyman and Yu [22] contains a brief summary, including references, of the most popular methods used today.

In the present work the generalized discrete variable representation (GDVR) method [23], developed in our group, has been used. It has previously been successfully applied to the OH+Cl [24] and CH_3+HBr [25] reac-

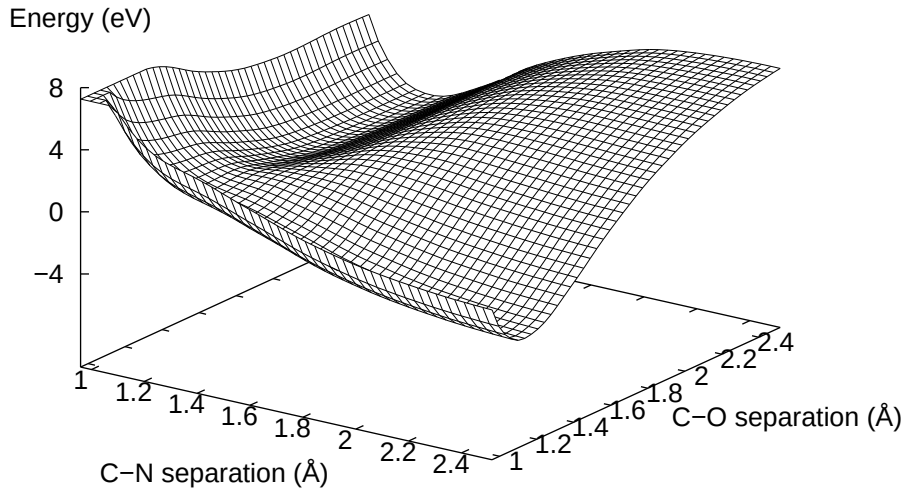

Figure 3.1: The collinear $^4\Sigma^-$ surface for the O+CN reaction, representing a typical potential energy surface. The surface is interpolated by GDVR from 484 energy points, of which 171 are CASPT2 ab initio energy points.

tions and to create a 3D potential energy surface for the HCBr molecule [26].

3.6 Spin-Orbit Interaction

So far we have only been concerned with non-relativistic quantum mechanics. Spin-orbit coupling, however, requires a relativistic treatment of the atom. This is far beyond the scope of this text, and fortunately spin-orbit coupling can at least be introduced by a much simpler semi-classical treatment.

From classical mechanics we know that a magnetic dipole moving in an electrostatic field will experience a force proportional to its velocity and the strength of the field. If we consider an electron moving in a central field, for example the effective potential energy of an unpaired electron moving around an atom, there will a coupling between the magnetic moment of the electron, and its orbital movement. This effect is called spin-orbit coupling, and will shift the energy up or down, depending on the sign of the spin of the electron.

This rather naive model of spin-orbit coupling can still give qualitative in-

sight in the properties of the spin-orbit interaction. With the help of classic electromagnetic theory, it can be shown that the spin-orbit coupling contribution to the total energy is proportional to $\boldsymbol{L}\cdot\boldsymbol{S}$, where $\boldsymbol{L}$ and $\boldsymbol{S}$ are the electronic orbital and spin angular momenta, which is the same relation given by the full relativistic treatment (see for example [27]). The presence of spin-orbit interaction leads to a break-down of the Born-Oppenheimer approximation, as the system is no longer defined by discrete, separated states. Instead, we have coupled states, where the system may jump between states, jumps that normally, in the absence of spin-orbit interaction, are spin-forbidden.

Chapter 4

Time Propagation

4.1 Classical Dynamics

4.1.1 Quasiclassical Trajectories

Classical trajectory calculations are the computationally cheapest method for studying reaction dynamics. In many cases trajectory calculation is the only available option, as quantum dynamics is generally not feasible except for small and light systems. A trajectory is defined as the set of position and momentum coordinates of a moving point as a function of time. By following this trajectory, the time evolution of the reaction can be studied (Fig. 4.1).

In classical trajectory dynamics, Newton's equations of motion,

$$-\frac{\partial V}{\partial q_i} = m_i \frac{d^2 q_i}{dt^2} \tag{4.1}$$

are solved for a set of initial conditions of the system. The solution to Eq. 4.1 is the path that the system will follow on the potential energy surface V. The main difficulties in classical trajectory calculations are finding the potential energy surface of the system, as described in the previous chapter, sampling the initial conditions, and choosing an appropriate integrator for solving Newton's equations of motion [28].

The difference between classical and quasiclassical trajectory calculations (QCT), is the inclusion of zero point energy, which is a purely quantum effect, in the initial conditions of QCT. This inclusion of the zero point energy generally gives better agreement with quantum calculations than pure classical trajectory calculations. Except for large systems, QCT is the standard method for investigation of reaction dynamics [29].

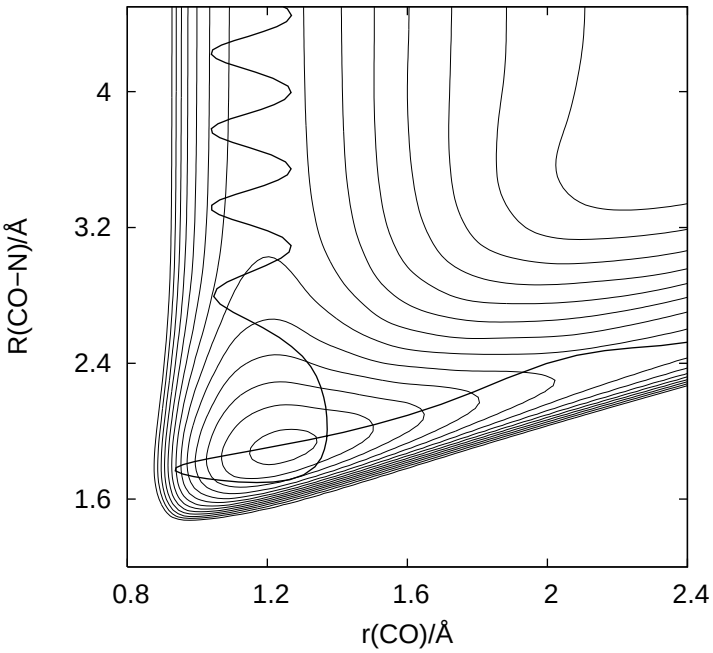

Figure 4.1: A quasiclassical trajectory. The trajectory illustrates the process $O + CN(v = 0) \rightarrow N + CO(v' = 2)$ on the collinear $^2\Pi$ potential energy surface.

4.1.2 Trajectory Surface Hopping

When two potential energy surfaces are coupled, through for example spin-orbit coupling, trajectory surface hopping (TSH) calculations can be used to allow the trajectory to jump between the surfaces. The methodology used here is based on the formulation given by Stine and Muckerman [30–32], where the dynamics is carried out on the adiabatic surfaces. When the two surfaces are sufficiently close, Landau-Zener theory [30] is used to determine if the system will undergo a non-adiabatic transition, that is, jump between the two adiabatic surfaces.

4.2 Wave Packet Dynamics

In wave packet dynamics a wave packet is propagated on a potential energy surface by solving the time-dependent Schrödinger equation,

$$i\hbar\frac{\partial}{\partial t}\Psi(\mathbf{r},t) = \hat{H}\Psi(\mathbf{r},t) \tag{4.2}$$

where the Hamiltonian operator is given by

$$\hat{H} = \hat{T} + \hat{V} = -\frac{\hbar^2}{2\mu}\nabla^2 + V(\mathbf{r}). \tag{4.3}$$

In Eq. 4.3, the potential $V(\mathbf{r})$ is obtained by solving Eq. 3.3 for each nuclear position $\mathbf{r}$. The formal solution to Eq. 4.2 is

$$\Psi(t) = \hat{U}(t, t_0)\Psi(t_0) \tag{4.4}$$

where $\hat{U}$ is the time-evolution operator, given by

$$\hat{U}(t, t_0) = \mathrm{e}^{-i\hat{H}(t-t_0)\hbar} \tag{4.5}$$

provided that the Hamiltonian is explicitly time-independent. The Hamiltonian $\hat{H}$ is an operator, making the time-evolution operator $\hat{U}$ an exponential function of an operator, which cannot be applied directly, since the potential and kinetic energy operators in the Hamiltonian do not commute ($\hat{T}\hat{V} \neq \hat{V}\hat{T}$).

4.2.1 The Wave Packet

In this project, where the NCO system is studied for collinear geometries, the time-dependent wave packet calculations were carried out in mass-weighted product Jacobi coordinates $(\tilde{R}, \tilde{r})$, using the Hamiltonian

$$\hat{H} = -\frac{\hbar^2}{2\mu}\left(\frac{\partial^2}{\partial\tilde{R}^2} + \frac{\partial^2}{\partial\tilde{r}^2}\right) + V(\tilde{R}, \tilde{r}), \tag{4.6}$$

where $\tilde{R}$ is the mass-weighted center-of-mass separation between N and CO, $\tilde{r}$ is the mass-weighted CO bond distance, and the reduced mass μ is given by

$$\mu = \left(\frac{m_\mathrm{O} m_\mathrm{C} m_\mathrm{N}}{m_\mathrm{O} + m_\mathrm{C} + m_\mathrm{N}}\right)^{1/2}. \tag{4.7}$$

The product Jacobi coordinates are given by

$$R = \alpha^{-1}\tilde{R}, \tag{4.8}$$

$$r = \alpha\tilde{r}, \tag{4.9}$$

where $\alpha = (\mu_R/\mu_r)^{1/4}$ and μ_R and μ_r are the reduced masses corresponding to the N-CO and CO systems, respectively. The initial wave packet is set up in reactant Jacobi coordinates, as a product of a vibrational eigenfunction of

the CN system, $\phi(r_{\mathrm{CN}})$, and a translational function in the form of a Gaussian wave packet, $\chi(R_{\mathrm{O-CN}})$,

$$\Psi(R_{\mathrm{O-CN}}, r_{\mathrm{CN}}, t = 0) = \phi_v(r_{\mathrm{CN}})\chi(R_{\mathrm{O-CN}}). \tag{4.10}$$

The wave function is then transformed to product Jacobi coordinates before the propagation begins. The vibrational eigenfunctions needed for the initialization and analysis are obtained by solving the time-independent Schrödinger equation for the diatomic fragments using a sine-basis expansion of the wave function. Fig. 4.2 shows examples of two initial wave packets for $\mathrm{CO}(\mathrm{X}^1\Sigma^+)$.

4.2.2 Split Operator Method with Fast Fourier Transforms

There are several methods for solving the time-dependent Schrödinger equation. A detailed discussion of these can be found in e.g. ref. [33]. The method used throughout our studies is the (second order) split-operator method, with fast Fourier transforms [34]. In this method the time-evolution operator is approximated by a splitting of the Hamiltonian. The Hamiltonian can be split such that the kinetic energy operator is between potential energy operators, referred to as the *kinetic referenced* split operator method,

$$\mathrm{e}^{-i(\hat{T}+\hat{V})\Delta t/\hbar} = \mathrm{e}^{-i\hat{V}\Delta t/2\hbar}\mathrm{e}^{-i\hat{T}\Delta t/\hbar}\mathrm{e}^{-i\hat{V}\Delta t/2\hbar} + O(\Delta t^3). \tag{4.11}$$

The validity of Eq.4.11 can be proved by Taylor expanding the left and right sides. The approximated time-evolution operator, Eq. 4.11, is Hermitian. It also conserves the norm of the propagated wave packet, which is an important property of the wave packet.

Choosing between kinetic referenced split operator method, shown in Eq 4.11, or the *potential referenced* split operator method, where the potential energy operator is between kinetic energy operators,

$$\mathrm{e}^{-i(\hat{T}+\hat{V})\Delta t/\hbar} = \mathrm{e}^{-i\hat{T}\Delta t/2\hbar}\mathrm{e}^{-i\hat{V}\Delta t/\hbar}\mathrm{e}^{-i\hat{T}\Delta t/2\hbar} + O(\Delta t^3), \tag{4.12}$$

is a matter of choice. Throughout this study, we have employed the kinetic referenced split operator method.

To solve the Schrödinger equation, the Hamiltonian has to operate on the wave packet at each time step. The potential part of the Hamiltonian is trivial, as it is local, *i.e.* the wave packet Ψ only has to be multiplied by the exponent of the potential energy V at each grid point. The kinetic part of the Hamiltonian involves a Laplacian operator (∇^2), which is a non-local operator in coordinate space. By transforming the wave packet to momentum space,

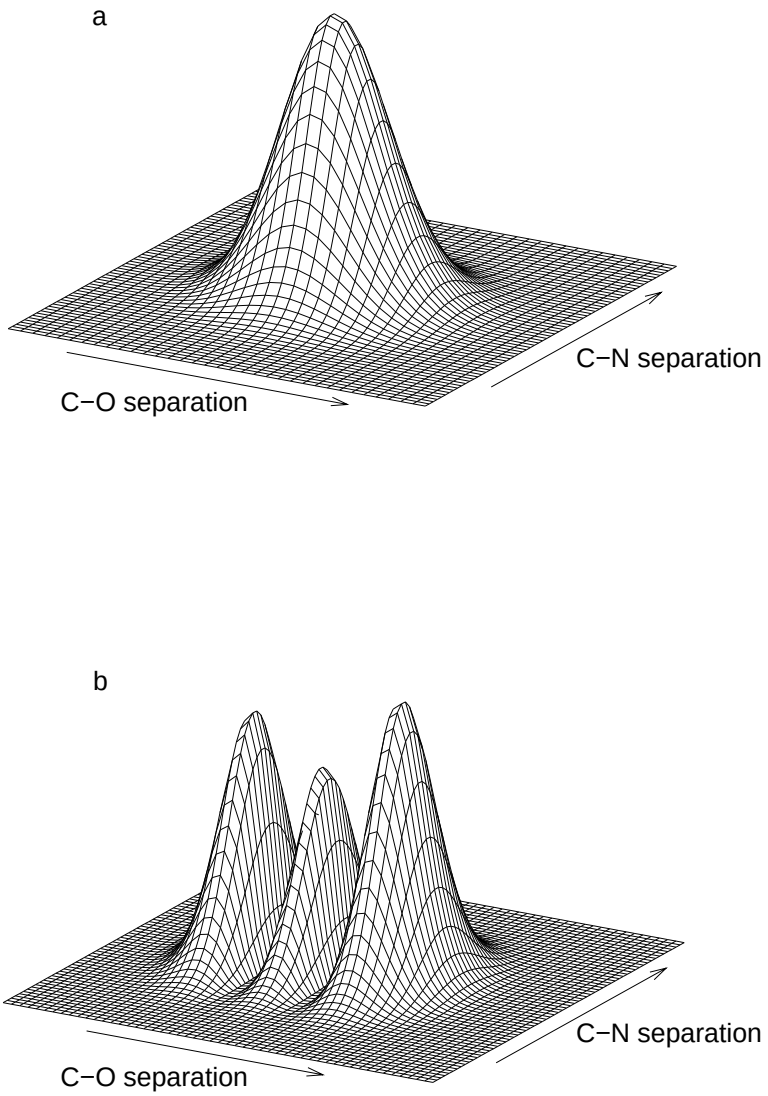

Figure 4.2: Wave packets according to Eq. 4.10 for $CO(X^1\Sigma^+)$ in the (a) vibrational ground state and (b) second exited state.

via a Fourier transform, the Laplacian can be evaluated as a local operator. The Fourier transform $\hat{F}$ is defined as

$$\hat{F}(\Psi) = \phi(k) = \frac{1}{\sqrt{2\pi}} \int_{-\infty}^{\infty} \mathrm{d}x \Psi(x) \mathrm{e}^{-ikx} \tag{4.13}$$

and the inverse Fourier transform $\hat{F}^{-1}$ as

$$\hat{F}^{-1}(\phi) = \Psi(x) = \frac{1}{\sqrt{2\pi}} \int_{-\infty}^{\infty} \mathrm{d}k \phi(k) \mathrm{e}^{ikx}. \tag{4.14}$$

It can easily be shown that the second order derivative of the wave function can be written as

$$\frac{d^2\Psi(x)}{dx^2} = \frac{1}{\sqrt{2\pi}} \int_{-\infty}^{\infty} \mathrm{d}k \phi(k) (ik)^2 \mathrm{e}^{ikx}. \tag{4.15}$$

It is seen that the second order derivative is a simple multiplication by $(ik)^2$ in momentum space. To evaluate the discrete Fourier transform, the fast Fourier transform algorithm [34] is used.

The algorithm for propagating the wave packet using the kinetic referenced split operator method is as follows: First the wave function is multiplied by $\mathrm{e}^{-\mathrm{i}\hat{\mathrm{V}}\Delta\mathrm{t}/2\hbar}$. This new function is Fourier transformed to momentum space and multiplied by the free particle operator $\mathrm{e}^{-\mathrm{i}\Delta\mathrm{t}\mathrm{k}^2\hbar/2\mu}$. An inverse Fourier transform is applied, and finally the function is again multiplied by $\mathrm{e}^{-\mathrm{i}\hat{\mathrm{V}}\Delta\mathrm{t}/2\hbar}$, which completes the time step. Thus, each time step involves one Fourier transform, one inverse Fourier transform and three simple multiplications. Using the fast Fourier transform, the scaling with grid-size is in the order of $N \log N$.

4.2.3 Damping Function

The discrete Fourier transform requires the function to be periodic. Therefore the wave packet has to be damped, if the wave packet is not to pass through the boundaries of the grid and reappear at the other end. When the wave packet reaches the end of the grid, it can also be nonphysically reflected from the boundary. These effects are avoided by damping the wave function (Fig. 4.3) between a point r_d and the boundary of the grid, r_max, in each coordinate:

$$f(r_i) = \begin{cases} 1, & r_i < r_\mathrm{d}, \\ \exp\left[-V_\mathrm{d}\Delta t/\hbar\right], & r_i \geq r_\mathrm{d} \end{cases}, \tag{4.16}$$

where V_d is the exponential damping function suggested by Vibók and Balint-Kurti [35]. We have also introduced a a time-dependent scale factor in the exponential damping function V_d, to account for the variation of the average product kinetic energy with time.

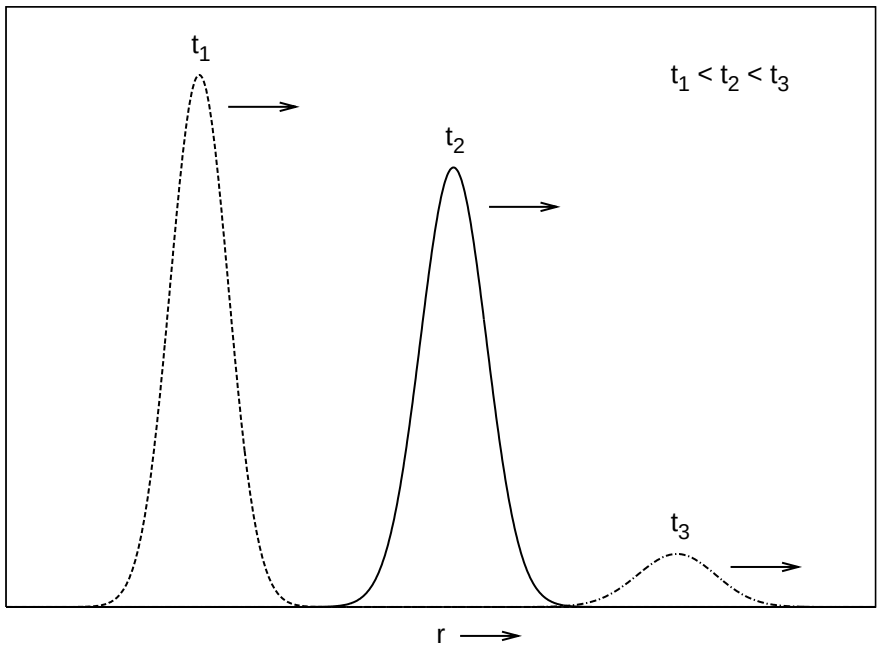

Figure 4.3: A wave packet is damped as it propagates through the damping region.

4.2.4 Analysis of the Scattered Wave Packet

The time propagation of the wave packet does not give much information in itself. The really interesting information is the state-to-state reaction probabilities. We start the wave packet in a given vibrational state (Eq. 4.10), so we get the probability for going from *one given* vibrational state in the reaction configuration to *all* vibrational states in the product configuration. These probabilities are found by, at a point R_{p}, before applying the damping function, projecting the scattered wave packet onto asymptotic vibrational eigenstates $\phi_{v'}(r)$:

$$c_{v'}(t) = \int \mathrm{d}r \phi_{v'}(r) \Psi(R_{\mathrm{p}}, r, t). \tag{4.17}$$

The time-dependent amplitudes $c_{v'}$ are Fourier transformed to energy space

$$b_{v'} = \frac{1}{\sqrt{2\pi}} \int \mathrm{d}t c_{v'}(t) \exp\left(iEt/\hbar\right), \tag{4.18}$$

and the state-to-state reaction probabilities (Fig. 4.4) are computed from the ratio between the scattered and incident fluxes [36],

$$P_{v \to v'}(E) = \frac{F_{v'}(E)}{F_v(E)}, \tag{4.19}$$

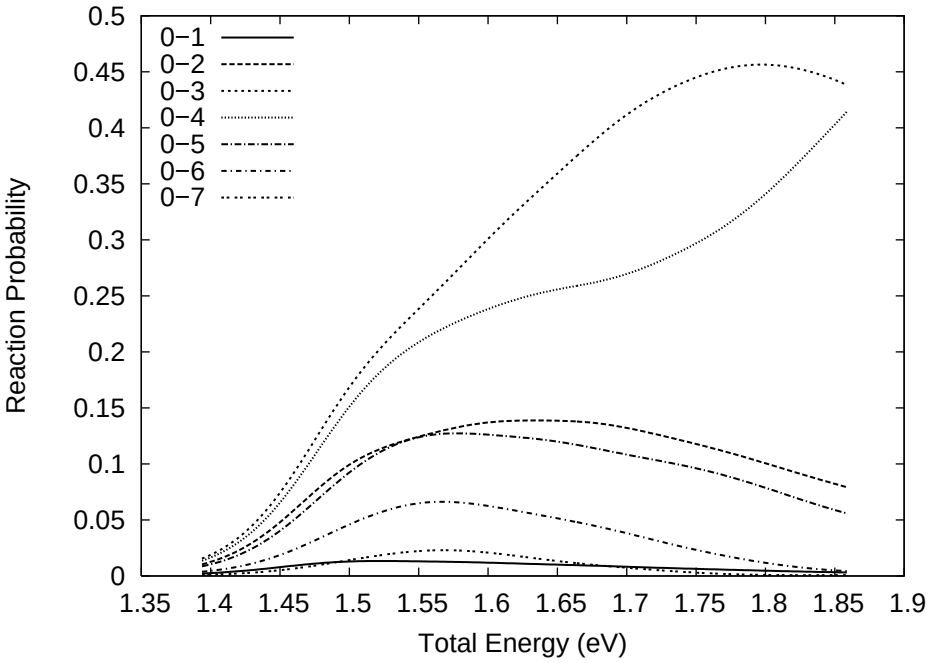

Figure 4.4: The state to state ($v - v'$) reaction probability for the collinear $O(^3P) + CN(X^2\Sigma^+) \rightarrow CO(X^1\Sigma^+) + N(^4S)$ reaction. The wave packet is initiated in the vibrational ground state, $v = 0$. The same data is presented in a different manner in Paper I, Fig. 7.

where

$$F_{v'}(E) = \frac{1}{\mu_{\mathrm{OC-N}}} k_{v'} \mid b_{v'}(E)|^2 , \tag{4.20}$$

$$k_{v'} = \frac{1}{\hbar}\sqrt{2\mu_{\mathrm{OC-N}}(E - V(R_{\mathrm{p}}) - E_{v'})} . \tag{4.21}$$

To avoid dividing by values near zero in Eq. 4.19, the outgoing wave packet is analyzed in an energy interval corresponding to 95% of the energy distribution in the incident Gaussian.

The incident flux, $F_v(E)$, is, in principle, given by an analytical expression [36], but since the potential has not reached its true asymptotic value at the position of the initial wave packet, a small correction is needed. The correction to the Gaussian distribution, illustrated in Fig. 4.5, is simply to obtain the probability distribution of the incident k-values by propagating the initial Gaussian wave packet $\chi(R)$ backwards. This k-distribution is then used to normalize the scattered components, rather than the initial Gaussian distribution.

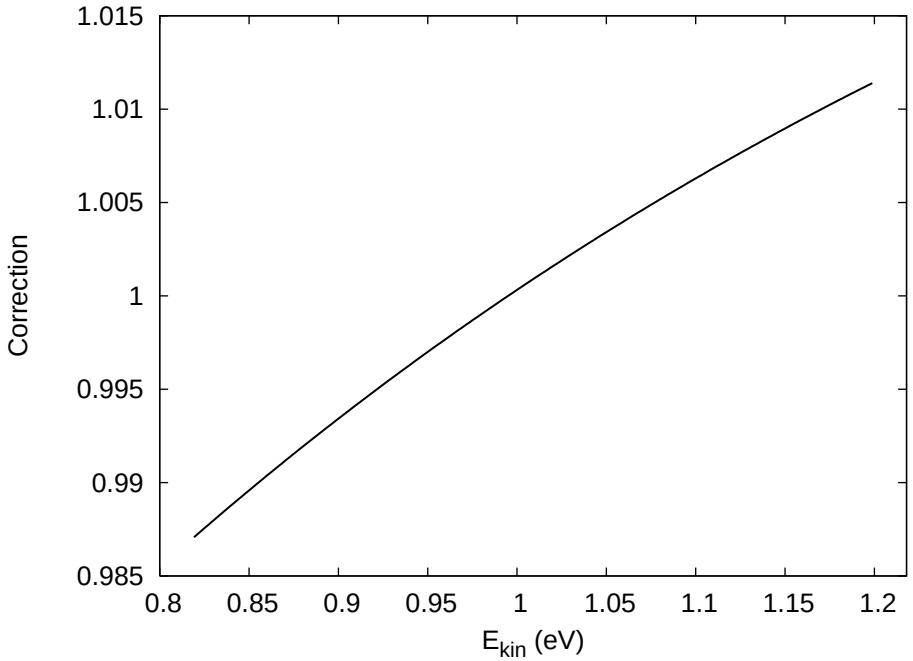

Figure 4.5: Example of a correction function. $\bar{E}_{\mathrm{kin}} = 1.0$ eV in the $\mathrm{O}(^3\mathrm{P}) + \mathrm{CN}(\mathrm{X}^2\Sigma^+)$ channel on the $^2\Pi$ surface.

4.2.5 Dynamics with Coupled Surfaces

In cases with two coupled potential electronic surfaces, as in Paper II, the Hamiltonian in (Eq. 4.6) must be changed, due to the fact that the potential energy operator now is a matrix:

$$\hat{V} = \begin{pmatrix} V_1 & V_{12} \\ V_{12}^* & V_2 \end{pmatrix}, \tag{4.22}$$

where V_1 and V_2 are the diabatic potential energy terms, and V_{12} are potential coupling terms. The Schrödinger equation now becomes

$$i\hbar \frac{\partial}{\partial t} \begin{pmatrix} \Psi_1 \\ \Psi_2 \end{pmatrix} = \left[\begin{pmatrix} \hat{T} & 0 \\ 0 & \hat{T} \end{pmatrix} + \begin{pmatrix} V_1 & V_{12} \\ V_{12}^* & V_2 \end{pmatrix} \right] \begin{pmatrix} \Psi_1 \\ \Psi_2 \end{pmatrix}. \tag{4.23}$$

In order to solve Eq. (4.23), the potential energy matrix has to be diagonalized at each grid point by the unitary transformation

$$\boldsymbol{D} = \boldsymbol{U}^\dagger \boldsymbol{V} \boldsymbol{U}, \tag{4.24}$$

where $\boldsymbol{D}$ is diagonal. The diagonal elements of the matrix $\boldsymbol{D}$ form two non-crossing, adiabatic surfaces. The exponential function of the matrix $\boldsymbol{V}$ can

now be written as

$$\mathrm{e}^{\boldsymbol{V}} = \boldsymbol{U}\mathrm{e}^{\boldsymbol{D}}\boldsymbol{U}^{\dagger}, \tag{4.25}$$

and the split-operator method can be used to propagate the wave packet on the two coupled electronic surfaces.

Chapter 5

Results and Discussion

5.1 Paper I

In Paper I we present CASPT2 calculations on the lowest collinear $^2\Pi$ and $^4\Sigma^-$ potential energy surfaces for the NCO system, corresponding to the $O + CN \rightarrow N + CO$ reaction. The potential energy surfaces are interpolated using the GDVR method. Both surfaces are exothermic, with an energy difference of 0.81 eV for the $^2\Pi$ and 3.39 eV for the $^4\Sigma^-$ surface. While the $^2\Pi$ surface has a 5.85 eV deep potential well, the $^4\Sigma^-$ surface exhibits a potential barrier of 1.42 eV.

Time-dependent wave packet calculations using the split-operator propagator have been performed on both surfaces in product Jacobi coordinates. The results on the $^2\Pi$ surface show structure in the reaction probabilities as a function of energy up to about 0.5 eV translational energy. On the $^4\Sigma^-$ surface the reaction is highly vibrationally non-adiabatic with initial translational energy more efficient in promoting the reaction than initial vibrational excitation. For reaction out of $v = 0$ the wave packet results show a systematic trend of increasing reaction probabilities for increasing product vibrational excitation up to $v' = 3$, thereafter the reaction probabilities decrease with further increasing product vibrational excitation. For reaction out of $v = 1$ and $v = 2$ these systematic trends are not observed. The wave packet calculations are compared to quasiclassical trajectory calculations. Generally the agreement is good, as would be expected. But differences in the product vibrational distributions primarily appear from reaction out of $v = 0$, which is related to the significant difference in initial classical and quantum distributions for $v = 0$.

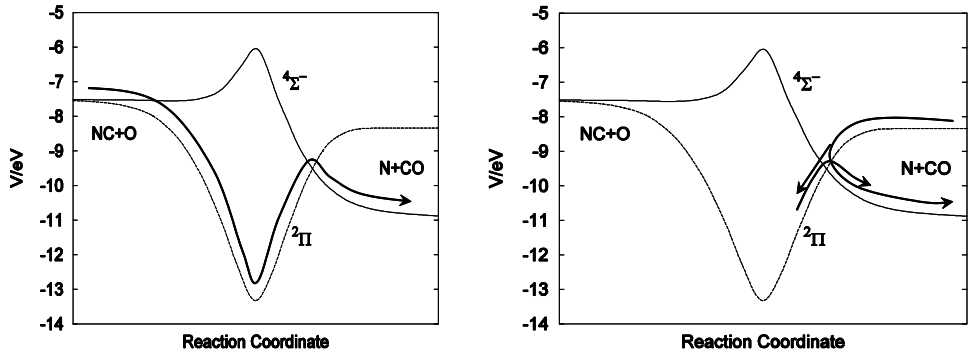

Figure 5.1: The possible pathways for transition from the $^2\Pi$ to the $^4\Sigma^-$ surface for the O + CN → N + CO reaction (left) and the non-reactive scattering of N+CO (right)

5.2 Paper II

In Paper II spin-orbit coupling between the two collinear $^2\Pi$ and $^4\Sigma^-$ potential energy surfaces for the NCO system are presented. The spin-orbit couplings are calculated using the RASSI method with CASSCF wave functions as basis set. The full spin-orbit coupling surface is interpolated using the GDVR method. The spin-orbit coupling is relatively strong in the asymptotic O+CN region, reaching a maximum of 0.007 eV before the crossing of the two potential energy surfaces. At the crossing the spin-orbit coupling is about 0.004 eV.

Wave packet calculations and TSH calculations on the coupled surfaces are presented for both the O + CN → N + CO reaction and the non-reactive scattering process N + CO → N + CO. The two cases are shown in Fig. 5.1, where the possible adiabatic pathways are illustrated.

In the former case, O+CN can react and form ground state CO and nitrogen in either the ground state (N(^{4}S)) or in the first excited state (N(^{2}D)). The energies studied are considerably lower than the potential energy barrier on the $^4\Sigma^-$ surface. Thus, all reactive processes have to enter the potential well of the $^2\Pi$ surface. After the potential well, the two surfaces cross, and spin-orbit coupling can allow transitions between the surfaces. Both the wave packet and the TSH calculations agree that this probability is low, about 0.05%, and has weak energy dependence, with slightly higher transition probabilities at lower energies.

The non-reactive scattering process N + CO → N + CO is initiated in the N(^{2}D) + CO channel on the $^2\Pi$ surface with kinetic energies below 0.7 eV, to avoid the formation of CN + O. The system can either stay on the diabatic

$^2\Pi$ surface, returning to the $N(^2D) + CO$ state, or it can transfer to the $^4\Sigma^-$ surface, and exit in the ground state $N(^4S) + CO$ channel. The TSH calculations show strong energy dependence in the transition probabilities. For energies below approximately 0.35 eV, the probability of crossing over to the lower diabatic surface, producing ground state nitrogen, is over 15%, while higher energies only allows the creation of a few percent ground state nitrogen. The wave packet calculations result in an average probability of around 0.5%. However, the transition probability shows a distinct resonance pattern, with peaks reaching a transition probability of about 10%. The wave packet calculations also show energy dependence in the transition probability, with larger peaks at lower energies, thus following the trend of the TSH calculations.

Chapter 6

Future and Outlook

Preliminary ab initio calculations on the lowest three dimensional $^4A''$ surface has shown that the collinear configuration might not be the most realistic path to form ground state nitrogen from CN and O. Thus, the next logical step in the investigation of the NCO system is to calculate the full three dimensional potential energy surface for the $^4A''$ state using CASPT2, and make an analytical fit of the ab initio energy points using the MBE method.

This potential energy surface is to be used to perform 3D QCT calculations, as well as 3D wave packet calculations. This would be feasible for at least $J = 0$. Such a study would attempt to explain the experimental results for the $O + CN \rightarrow CO + N$ reaction.

The $^2A'$ and $^2A''$ surfaces have previously been presented. The combination of three heavy atoms and a deep potential well makes the system very interesting, and wave packet calculations nearly impossible. Previous 2D wave packet calculations, both by us and other groups, have shown that there are quantum effects present, even for the heavy NCO system, in the collinear configuration. It would be very interesting to perform full dimensional wave packet calculations on these surfaces and compare the result with the collinear and classical studies.

In this and previous studies of the NCO system, the Renner-Teller effects have been neglected. The Born-Oppenheimer approximation breaks down due to the degenerate ground states, and it is possible that these effects would affect the dynamics of the system, by allowing intersurface crossing. These effects should be studied.

There are several excited states of the NCO system that has not been investigated. Non-adiabatic processes, such as spin-orbit coupling, could facilitate reaction pathways previously undiscovered. The first task would be to study the coupling between the ^2A and the $^4A''$ states, followed by calculations of other excited states.

Bibliography

[1] M. Simonson, N. Marković, S. Nordholm, B. Persson, Chem. Phys. 200 (1995) 141.

[2] S. Andersson, N. Marković, G. Nyman, J. Phys. Chem. 107 (2003) 5439.

[3] E. Herbst, W. Klemperer, Astrophys. J. 185 (1973) 505.

[4] E. Herbst, H.-H. Lee, D. Howe, T. Millar, Mon. Not. R. Astron. Soc. 268 (1994) 335.

[5] G. D. Forêtes, E. Roueff, D. Flower, Mon. Not. R. Astron. Soc. 244 (1990) 668.

[6] S. Federman, C. Strom, D. Lambert, J. Cardelli, V. Smith, C. Joseph, Astrophys. J. 424 (1994) 772.

[7] M. Gerin, Y. Viala, F. Pauzat, Y. Elliinger, Astron. Astrophys. 266 (1992) 463.

[8] M. Monnerville, P. Halvick, J. Rayez, J. Chem. Soc. Faraday Trans. 89 (1993) 1579.

[9] M. Monnerville, G. Peoux, S. Briquez, P. Halvick, Chem. Phys. Lett. 322 (2000) 157.

[10] A. Abrol, L. Wiesenfeld, B. Lambert, A. Kuppermann, J. Chem. Phys. 114 (2001) 7461.

[11] C. Schulz, H.-R. Volpp, J. Wolfrum, Chemical Dynamics in Extreme Environments, World Scientiffic, Singapore, 2001, p. 206.

[12] K. J. Schmatjko, J. Wolfrum, J. Ber. Bunsenges. Phys. Chem. 79 (1975) 696.

[13] K. J. Schmatjko, J. Wolfrum, J. Ber. Bunsenges. Phys. Chem. 82 (1978) 419.

[14] C. J. Cobos, React. Kinet. Catal. Lett. 57 (1996) 43.

[15] T. Helgaker, P. Jørgensen, J. Olsen, Molecular Electronic-Structure Theory, Wiley, Chichester, 2000.

[16] C. Møller, M. S. Plesset, Phys. Rev. 48 (1934) 618.

[17] C. J. Cramer, Essentials of Computational Chemistry, Wiley, 2002.

[18] B. O. Roos, Chem. Phys. 66 (1982) 197.

[19] S. Andersson, N. Marković, G. Nyman, Phys. Chem. Chem. Phys. 2 (1999) 613.

[20] S. Sato, J. Chem. Phys. 23 (1955) 592.

[21] J. Murrell, S. Carter, S. Farantos, P. Huxley, A. Varandas, Molecular Potential Energy Surfaces, Wiley, Chichester, 1984.

[22] G. Nyman, H.-G. Yu, Rep. Prog. Phys. 63 (2000) 1001.

[23] H. G. Yu, S. Andersson, G. Nyman, Chem. Phys. Lett. 321 (2000) 275.

[24] H. G. Yu, G. Nyman, J. Chem. Phys. 113 (2000) 8936.

[25] H.-G. Yu, G. Nyman, J. Chem. Phys. 105 (2001) 2240.

[26] H.-G. Yu, T. Gonzales-Lezana, A. Marr, J. Muckerman, T. Sears, J. Chem. Phys. 115 (2001) 5433.

[27] Modern Quantum Mechanics Rev.Ed., Addison Wesley, Reading, 1994.

[28] L. M. Raff, D. L. Thompson, Theory of Chemical Reaction Dynamics, Volume III, CRC Press, Boca Raton, 1985.

[29] F. J. Aoiz, L. Bañares, V. J. Herrero, J. Chem. Soc. Faraday Trans. 94 (1998) 2483.

[30] J. Stine, J. Muckerman, J. Chem. Phys. 65 (1976) 3975.

[31] J. Stine, J. Muckerman, J. Chem. Phys. 68 (1978) 185.

[32] R. Preston, J. Tully, J. Chem. Phys. 54 (1971) 4297.

[33] C. Leforestier, R. H. Bisseling, C. Cerjan, M. D. Feit, R. Friesner, A. Guldberg, A. Hammerich, G. Jolicard, W. Karrlein, H. D. Meyer, N. Lipkin, O. Roncero, R. Kosloff, J. Comput. Phys. 94 (1991) 59.

[34] D. Kosloff, R. Kosloff, Comput. Phys. Letters 173 (1983) 35.

[35] Á. Vibók, G. G. Balint-Kurti, J. Phys. Chem. 96 (1992) 8712.

[36] N. Marković, G. D. Billing, J. Chem. Phys. 100 (1994) 1085.